

Supporting Information for "North Atlantic and Pacific quasi-stationary parts of atmospheric rivers and their implications for East Asian monsoon onset"

Hung-I Lee¹, Jonathan L. Mitchell^{1,2}, Aradhna, Tripathi^{1,2,3,4}, Juan M.

Lora^{2,5}, Gang Chen¹, and Qinghua Ding^{6,7}

¹Department of Atmospheric and Oceanic Sciences, University of California, Los Angeles, California, 90095, USA

²Department of Earth, Planetary, and Space Sciences, University of California, Los Angeles, California, 90095, USA

³Institute of the Environment and Sustainability, University of California, Los Angeles, California, 90095, USA

⁴European Institute of Marine Sciences (IUEM) Universit de Brest, UMR 6538, Domaines Ocaniques, Rue Dumont D'Urville, and

IFREMER Plouzan, France

⁵Department of Geology and Geophysics, Yale University, New Haven, Connecticut, 06511, USA

⁶Department of Geography, University of California, Santa Barbara, California, 93117, USA

⁷Earth Research Institute, University of California, Santa Barbara, California, 93117, USA

Contents of this file

1. Text S1 to S3
2. Figures S1 to S8
3. Tables S1 to S2

Text S1. Technique to smooth precipitation contours in Fig. 1 and Fig. 3 The key issue to smooth precipitation contours is the influence of precipitation from surface topography in East Asia. A series of precipitation spikes occur in East Asian and North American continents in Fig. S2. Once you perform the filtering without dealing with precipitation spikes, the effect of surface topography will spread out to the neighboring areas and distort the shapes of precipitation contours, so we need to remove the spikes of precipitation. We first smooth precipitation by filtering out the signals greater than the typical spectrum of topography ($\sim 0.2 \text{ degree}^{-1}$) and then pick up the local minimum values of the curves. The final curve is obtained by cubic interpolation of each local minimum. Therefore, we can perform a special-temporal low-pass filtering (cutoff frequency $0.027 \text{ degree}^{-1}$ in this case) to smooth precipitation. Although the technique lowers the overall average of precipitation, the spatial-temporal pattern is preserved without the strong influence of spikes.

Text S2. Precipitation and CWV

Global precipitation and CWV at 30°N over global ocean basins for the past 39 years (1979-2017) has been displayed in Fig. S3 using ERA-Interim reanalysis. Since 40 mm CWV coincides with $5 \text{ mm}/d$ precipitation, the 40-mm exceedance criteria of CWV in QSAR pathways is a reasonable quantity.

Text S3. The sensitivity test of different window sizes, and the dateline crossing date

The QSAR tracking algorithm can be viewed as a low-pass filter especially for narrow window sizes. Since the typical size of an AR is about $3\text{-}5^\circ$ in longitude, those fluctuations

that have been filtered out are mainly inside the range of a QSAR. Hence, the tracking algorithm intrinsically smoothens QSAR pathways by filtering out inherent fluctuations inside QSARs.

The window size sensitivity of QSAR pathways could be reduced from 10° to 5° in longitude and the number of multiple crossing of the dateline by applying the tracking algorithm on 7-day running mean of CWV data. However, it also enhances the uncertainties of QSAR pathways by 7 days, and reduces the resolutions of QSAR pathways especially during monsoon onset periods. For example, the predicted QSAR pathway using daily CWV is closer to the eye-catching QSAR than the one using 7-day running mean CWV during mid-May, 2017 (Fig. S7). Hence, the QSAR pathway determined by 7-day running mean CWV blurs the exact EASM onset date. The usage of running mean with larger time period trades the accuracy of QSAR pathways and monsoon onset dates for lower window size sensitivities and numbers of multiple dateline crossings. To achieve a single QSAR dateline crossing requires performing the tracking algorithm on running mean CWV data for more than 7-days, and this further blurs the EASM onset date. Therefore, we avoid taking time mean of the data, and try to develop the dateline crossing index by only averaging over area.

Hence, this dateline crossing date index was constructed based on the fact that the migrations of QSAR cause zonal anomalies of Pacific CWV. During wintertime, the Eastern Pacific contains relatively larger CWV than the Western Pacific. As the QSAR moves into the Western Pacific in summer, the CWV is larger in the Western Pacific than in the Eastern Pacific (Fig. S8).

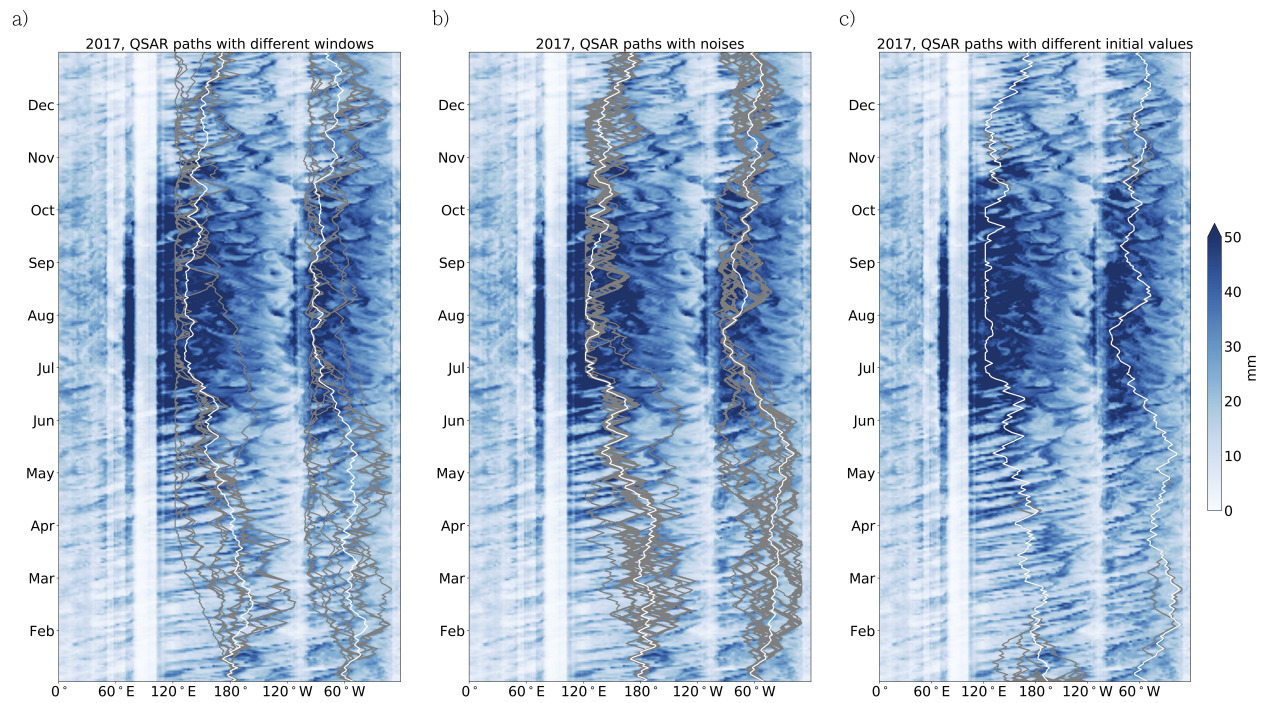


Figure S1. **a.** Hovmöller diagrams of CWV (2017) with simulated QSARs (grey curves) using different pairs of window sizes and their ensemble averages (white curves). **b.** Same as **a.**, but for one thousand realizations by adding white noise to the raw CWV. **c.** Same as **a.**, but for different initial longitudes of Pacific.

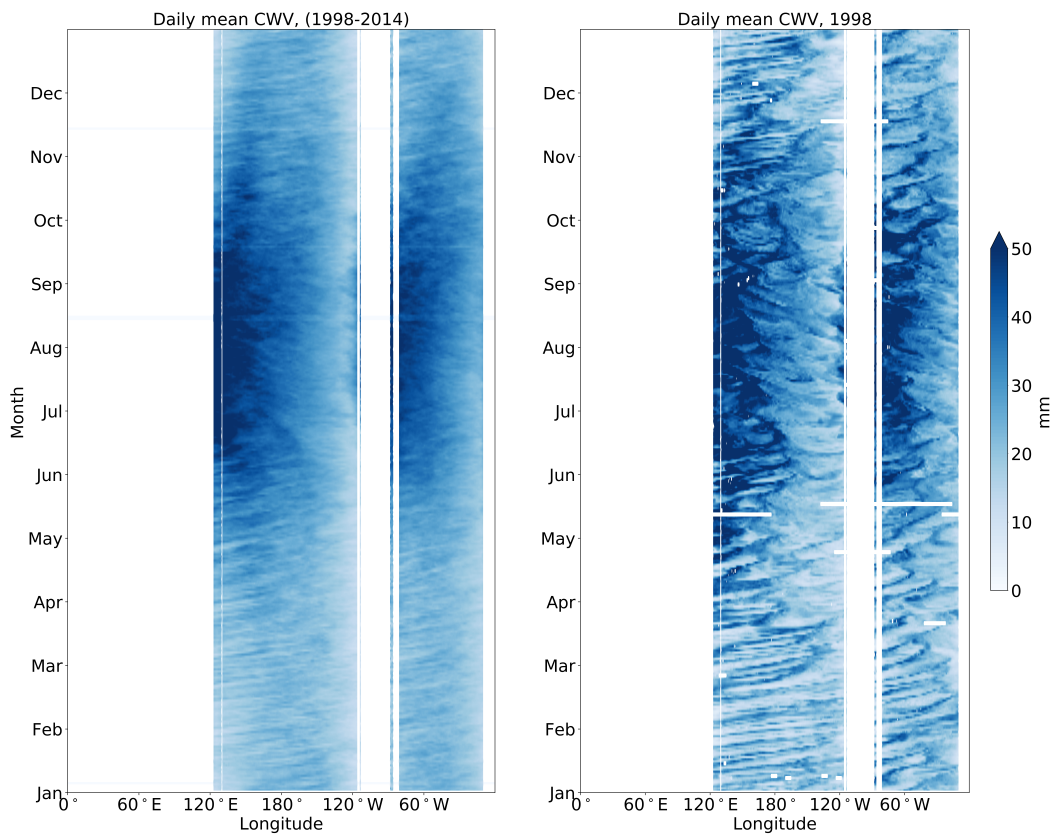


Figure S3. (Left) Hovmöller diagram of CWV in climatology mean (1998-2014) and (right) in 1998 using Tropical Rainfall Measuring Mission’s (TRMM) Microwave Imager (TMI) data. The QSARs are displayed the same as reanalysis data. However, to obtain more statistical analysis (1979-2017), we used ERA-Interim data.

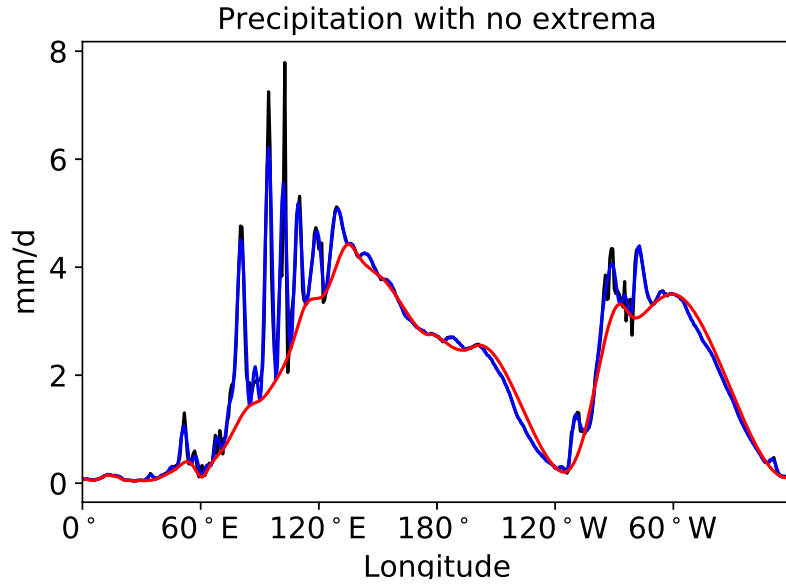


Figure S4. Annual mean of climatological (1979-2017) precipitation (the black curve). Primary filtering by removing high frequency (0.2 degree^{-1} in this case, the blue curve). The precipitation without spikes (the red curve).

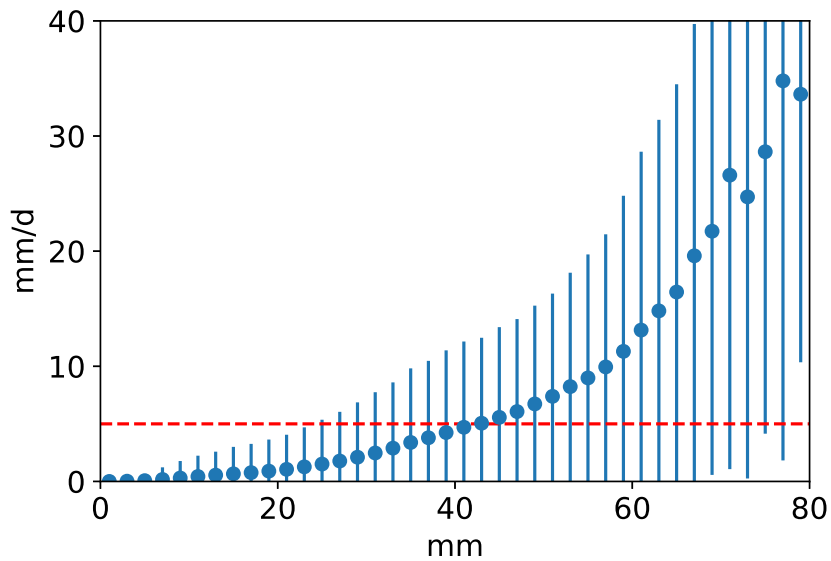


Figure S5. The averaged precipitations (blue dots) and standard deviations (blue error-bars) w.r.t. CWV at 30°N over global ocean basins for the past 39 years (1979-2017). The red dashed line shows the 5 mm/d precipitation.

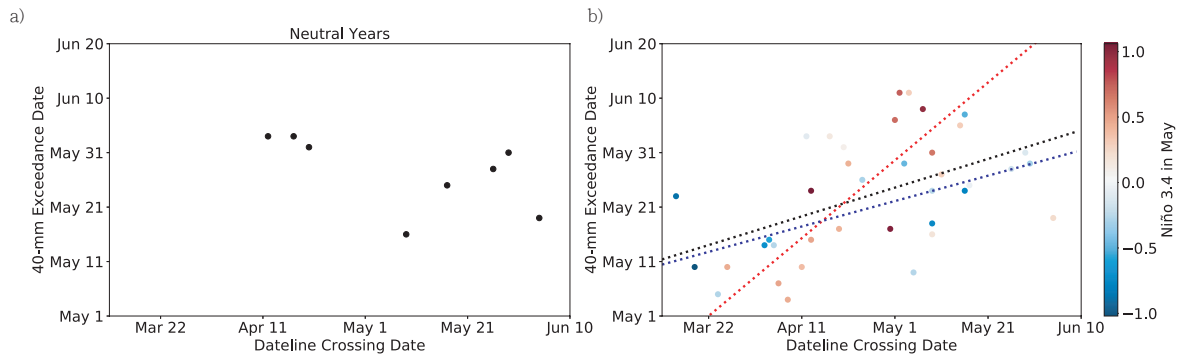


Figure S6. a. The scatter plot of 40-mm exceedance date of the QSAR, and the dateline crossing during neutral years. b. Same as a., but for entire past 39 years with the slope 0.26, intercept 112 days, correlation coefficient 0.51, and p-value 0.001 by linear regression analysis (as shown in the black line). Linear regression analysis of El Niño (the red line) and La Niña (the blue line) are added for comparison.

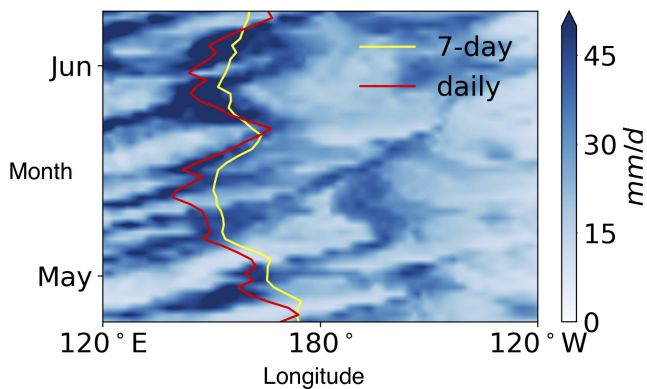


Figure S7. Hovmöller diagram of CWV (2017) at 30°N with the QSAR pathway identified for daily CWV (the red curve) and the QSAR pathway for 7-day running average CWV (the yellow curve).

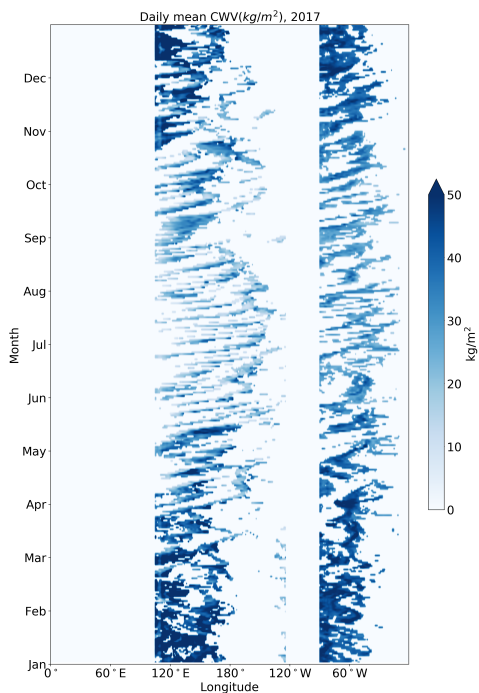


Figure S8. Hovmöller diagram of the Pacific CWV and Atlantic CWV (at 30°N in 2017) that are 1.15 times greater than the average CWV for each respective basin.

Table S1. The percentages of days with CWV local maxima occurring at window edges with different pairs of window sizes. °W/°E stands for a window size west/east of QSAR pathways at the previous day.

°W	°E	percentages (Pacific)	percentages (Atlantic)
2.25	2.25	68.8	57.3
2.25	3	68.2	61.6
3	2.25	65.5	55.1
3	3	63.0	52.9
3	3.75	60.8	51.8
3.75	3	56.7	45.8
3.75	3.75	55.1	51.8
3.75	4.5	55.9	50.1
4.5	3.75	54.8	41.1
4.5	4.5	53.7	41.4
4.5	5.25	51.0	39.7
5.25	4.5	54.8	38.1
5.25	5.25	51.0	39.5
5.25	6	49.6	34.2
6	5.25	46.3	36.2
6	6	43.8	30.1
6	6.75	42.5	28.5
6.75	6	41.4	30.4
6.75	6.75	38.9	27.1
6.75	7.5	37.8	26.3
7.5	6.75	41.4	27.4
7.5	7.5	38.4	24.4
7.5	8.25	36.7	20.8
8.25	7.5	37.3	24.7

Table S2. QSAR dateline crossing dates, first 40-mm CWV exceedance dates, dateline crossing lead-dates (the negative value mean lag-date), and Niño 3.4 in May.

Year	Dateline Crossing	40-mm Exceedance	Lead-Date	Niño 3.4
1979	Jun/4	May/19	-16	0.23 Neutral
1980	Apr/13	May/15	32	0.48 El Niño
1981	Apr/5	May/14	39	-0.26 La Niña
1982	May/9	May/31	22	0.66 El Niño
1983	Apr/13	May/24	41	1.06 El Niño
1984	May/16	Jun/7	22	-0.51 La Niña
1985	May/16	May/24	8	-0.78 La Niña
1986	May/29	May/31	2	-0.12 Neutral
1987	May/7	Jun/8	32	0.97 El Niño
1988	Mar/15	May/23	69	-0.88 La Niña
1989	Apr/4	May/15	41	-0.58 La Niña
1990	May/4	Jun/11	38	0.29 El Niño
1991	Mar/26	May/10	45	0.45 El Niño
1992	Apr/28	Jul/28 ^a	91	1.06 El Niño
1993	May/1	Jun/6	36	0.7 El Niño
1994	Apr/19	May/17	28	0.42 El Niño
1995	Apr/17	Jun/3	47	0.14 Neutral
1996	May/30	May/29	-1	-0.31 La Niña
1997	May/2	Jun/11	40	0.75 El Niño
1998	Apr/8	May/4	26	0.45 El Niño
1999	Mar/19	May/10	52	-1.02 La Niña
2000	Apr/3	May/14	41	-0.71 La Niña
2001	May/9	May/24	15	-0.25 Neutral
2002	Apr/21	May/29	38	0.43 El Niño
2003	May/5	May/9	4	-0.26 La Niña
2004	May/9	May/16	7	0.17 Neutral
2005	May/11	May/27	16	0.29 El Niño
2006	May/17	May/25	8	-0.05 Neutral
2007	Apr/24	May/26	32	-0.29 La Niña
2008	May/9	May/18	9	-0.75 La Niña
2009	Apr/20	Jun/1	42	0.09 Neutral
2010	Apr/12	Jun/3	52	-0.09 Neutral
2011	May/3	May/29	26	-0.47 La Niña
2012	May/26	May/28	2	-0.18 Neutral
2013	Mar/24	May/5	42	-0.27 La Niña
2014	May/15	Jun/5	21	0.3 El Niño
2015	Apr/30	May/17	17	1.02 El Niño
2016	Apr/6	May/7	31	0.48 El Niño
2017	Apr/11	May/10	29	0.38 El Niño

^a An outlier in 1992.